

Friction stir welding of AA2024 and AA2198 Aluminum alloys: effect of tool geometry and process parameters

Mahdi Masoumi¹, Yasser Zedan², Damien Texier³, Mohammad Jahazi⁴, and Philippe Bocher⁵

1. MSc. Student

2, 3. Research Assistant

4, 5. Professor

Aluminium Research Centre-REGAL, École de technologie supérieure, Montreal, Canada

Corresponding author: mahdimasoumi90@gmail.com

Abstract

In the present research an appropriate tool design is developed for joining of AA2198-T3 and AA2024-T3, subsequently the influence of rotational and traverse speed for the selected tool on the joint tensile properties is evaluated. Three shoulder profiles (flat, spiral, and fan) and five different pin profiles (tapered cylindrical, straight cylindrical, threaded cylindrical, cone, and square) were designed. The weld quality has been evaluated by means of visual inspection, microstructure analysis and tensile tests. Local strain maps measurements using Digital Image Correlation (DIC) enabled to determine weld local properties and determine the joints failure mode during monotonic tensile loading test. Two dimensional hardness map across the cross section through the weld joint was also carried out to further document the heterogeneities of the FSW joint. The tapered cylindrical pin with a fan shoulder was the optimal tool design configuration in terms of mechanical properties. Tensile tests were conducted on the joints produced by optimal tool design at different traverse and rotational speeds. The fracture of samples occurred in the HAZ of the advancing side (AA2198) and in the middle of the joint, which are zones depicting the highest strain values and the lowest hardness values via DIC technique and micro hardness measurements, respectively. Higher traverse speed was found to increase the joint yield strength. The joint efficiency can reach up to 78% by choosing optimum welding speed parameters of 750 rpm and 450 mm/min. Besides, it has been found that although the rotational speed has not a significant effect on the mechanical properties, higher rotational and traverse speeds can enhance the formation of tunneling and kissing bond defects in the joint.

Keywords: FSW tool design, friction stir welding, Al-Li alloys, welding speed, 2024 aluminum alloy.

1. Introduction

Recently developed aluminum alloys, such as the AA2198 Al-Li alloys, are materials of choice for lightweight structural applications due to improved mechanical properties and lower density compare to their conventional counterparts, e.g., AA2024 [1]. However, these benefits come at the expense of higher material costs. Therefore, an economical solution is to use hybrid designs with AA2198 alloys only for critical regions/components, with the remaining structure retaining AA2024 alloys. A method for joining these dissimilar materials is ultimately needed. Unfortunately, conventional fusion welding methods are not appropriate solutions as they result in welding defects, such as hot cracking [2].

Friction stir welding (FSW) is a solid-state welding technique that has evolved as a solution for joining dissimilar materials that are difficult to weld [3]. It is currently used as an alternative to riveting for the assembly of airplane fuselages. FSW uses a rotary pin to locally mix the materials of the two sides of the joint below the melting point temperature. Thus, the formation of welding defects such as hot cracking is prevented.

Selecting appropriate FSW tool and process parameters is essential for producing reliable joints for aerospace applications, especially for joining dissimilar alloys with different mechanical and thermal properties. Both the shoulder and pin profiles are important for having a defect-free joint. The optimization of either the shoulder [4-6] or the pin design [7-11] for FSW tools has been reported in the literature for producing joints with higher mechanical properties. L. Trueba Jr. *et al.* [6] showed that the fan shoulder has a significant potential for producing high quality welds, even under non-ideal process conditions. K. Krasnowski [12] showed that cylindrical pins with and without thread are capable of producing defect-free joints for AA6082-T6 aluminum alloys. The effect of the pin geometry on the mechanical properties of FSWed AA2014 aluminum alloy was also reported by Zhao *et al.* [13]. They found that the optimum weld quality was obtained by using the taper pin with a screw thread.

In the light of the fact that the last generation of aluminum are relatively new materials, the optimization of tool design and welding speed for these materials requires particular investigations. Bitindo *et al.* [14] studied welding parameters on the combined optimization of the yield stress and the tensile strength of FSWed AA2198-T3 butt joints. Their multi-objective optimization methods indicate that best quality joints can be manufactured by using their suggested optimal conditions of 531 rpm and 300 mm/min for rotational and welding speed, respectively.

However, these optimized welding parameters were obtained from empirical model and have not proved it experimentally. Radisavljevic [15] worked on joining of AA2024-T3 and they have found that optimized conditions range from 750 to 950 rpm and from 73 to 193 mm/min.. According to the authors' knowledge, no research on optimization of friction stir welding tool geometry and parameters for joining dissimilar AA2024 and AA2198 joints was reported in the literature. Dissimilar friction stir welded butt joints made of AA2024-T3 and AA2198-T3 have been already been investigated in terms of microstructural and specific mechanical characterizations [16, 17]. In this study, the effect of tool shoulder and pin profile on the microstructure and mechanical properties of FSWed AA2024-T3/AA2198-T3 joints were documented after welding, without any natural aging. To that end, three different shoulder and five tool pin profiles were used to produce different joint variants, while the other welding parameters were kept constant to find the optimal tool design. To assess the influence of FSW welding speed on the mechanical properties of the joints, different traverse speeds in the range of 50 mm/min to 450 mm/min with two different rotational speeds of 750 and 1000 rpm by optimal tool design have been investigated.

2. Experimental Procedures

2.1. Tool design and material

The 49-HRC quenched-temper AISI 4340 were used as tool material [18]. Tool profile design for different tools has been chosen based on literature review as shown in Table 1. Seven tool configurations denoted from A to G in Figure 1 were designed and manufactured to evaluate the quality of the joint. Their dimensions are shown in Table 2.

Shoulder profile	Pin profile	Configuration
Spiral shoulder [18]		B
Raised fan shoulder [6]		C, D, E, F and G
	Stepped conical pin [19]	B and C
	Half-screw pin [20]	D
	Straight cylindrical pin [5]	E
	Square pin [21]	G

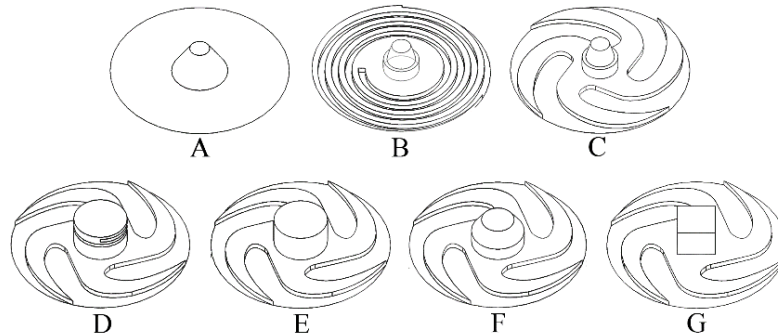


Figure 1. Tool configurations: (A) Flat shoulder with conical pin, (B) Spiral shoulder with stepped conical pin, (C) Fan shoulder with stepped conical pin, (D) Fan shoulder with threaded cylindrical pin, (E) Fan shoulder with cylindrical pin, (F) Fan shoulder with tapered cylindrical pin, (G) Fan shoulder with cubic pin.

Parameter	Dimensions (mm)	Types
Tool shoulder diameter	15.8 Ref. [18]	All
Pin length	2.7 Ref. [22]	All
Max outer pin diameter	3.2 Ref. [19]	A, B and C
	4.7 Ref. [18]	D, E, F and G
Min-pin diameter	1.6	A, B and C
	3.2	F

2.2. Materials and methods

The base materials AA2024-T3 and AA2198-T3 rolled sheets (thickness of 3.2 mm) were used in the present investigation. In the case of dissimilar joints, AA2024 and AA2198 plates were placed on the retreating side and on the advancing side, respectively. The weld was perpendicular to the AA2198 rolling direction and parallel to the AA2024 rolling direction as suggested in Ref. [16]. There are two goals in this project. The first goal is to find an appropriate tool geometry for friction stir welding of AA2024-T3 and AA2198-T3. To address this goal, the welding parameters were kept constant and different tool designs were tested. The rotation speed, the welding traverse speed, the plunge depth and tilt angle were 750 rpm, 50 mm/min, 0.2 mm and 0 degree, respectively. These selected parameters are close to advised parameters in Ref. [15]. It is worth mentioning that the low traverse welding speed guarantee that the weld is hot enough to avoid typical defects. In other words, defects -if there are – will be related to the tool design and not to process parameters. To ensure that the mismatch between plate edges has no effect on the formation of defects within the joints and any defects present would only be related to the tool design, all tools were first tested using the similar joint of AA2024-T3 plates. Tools that did not produce any defects such as kissing bonds, flash, and tunneling defects, on the basis of metallography and eye examination were selected for the dissimilar welding of AA2024 and AA2198. The second goal is to find the optimized welding speed range for the selected tool. Table 3 presents different traverse and rotational speeds of FSW process used for documenting the second goal of the present investigation.

To reveal the microstructure, Keller etchant for 15 seconds were employed after standard polishing down to 1 μm diamond paste and BUEHLER Vibromet2 for 48 h with 0.05 μm colloidal silica solution. Optical micrographs were obtained with an OLYMPUS Lext OLS4100 laser scanning confocal microscope. Mechanical characterizations were performed on dog-bone tensile specimens. They were machined from the welded plates so that the loading direction was parallel to the cross-welding direction of the joined plates. Specimens were extracted both from the joint (the joint being centered in the specimen gage) and from the base materials for references. Tensile tests were conducted on a 5kN Kammrath & Weiss micro-tensile device at a constant crosshead displacement rate of 7 $\mu\text{m}\cdot\text{s}^{-1}$; *i.e.* a strain rate of approximately $2.3\times 10^{-4}\text{ s}^{-1}$. The specimen elongation along the loading direction was continuously recorded using a Keyence LS-7030M optical extensometer sampling the extremities of the TMAZ regions ($L_0=16\text{mm}$). The tensile test has been repeated three times for each welding condition. Optical microscope images were simultaneously recorded for different loading conditions to calculate the local strain fields from measured displacement fields via optical high resolution-Digital image correlation technique (OHR-DIC) as explained in Ref. [17, 23]. Vickers hardness map was performed using an automatic microhardness machine (CLEMEX), with a 25gf load applied for 10s. To analyze the hardness distribution through a weld cross-section, 31 profiles of 260 indents have been made with an increment of 80 μm in the cross-weld and thickness directions.

Sample code	Rotational speed (rpm)	Traverse speed (mm/min)
$\omega 750V50$	750	50
$\omega 750V150$	750	150
$\omega 750V300$	750	300
$\omega 750V450$	750	450
$\omega 1000V300$	1000	300
$\omega 1000V450$	1000	450

3. Results

3.1. Tool selection for joining AA 2024-T3 and AA2198-T3

Metallography and visual examination results corresponding to the occurrence of kissing bond, tunneling defects and flash formation on the welded AA2024-T3 joints are summarized in Table 4. A flat shoulder (tool A) was shown to lead to flash formation on the welded surface because the flat shoulder has not any feature to bring back the material to the center during the rotation of tool. On the other hand, spiral and fan shoulders prevent the weld from flash defect formation. The tools used, having min-pin diameters half of the plate thickness (tools A, B and C), created kissing bond defects. When the min-pin diameter is equal to the plate thickness (tools D, E, F and G), no kissing bond defect is present. This phenomenon can be related to the fact that a bigger min-pin diameter provides enough material flow at the root of the weld to join the materials. The results of the half-threaded cylindrical pin (tool D) show a tunneling defect, which can be the result of high turbulent flow in the joint. Based

on this evaluation, only tools E, F and G were able to create defect-free joints, and they were selected for use in joining AA2024-T3 and AA2198-T3.

Cross-section observations of joints between AA2024-T3 and AA 2198-T3 produced by tools E, F and G are shown in Figure 2. They confirm that defect-free joints were obtained using tools E, F, and G. The microstructures of the base metals and joints are detailed in Ref. [16, 24].

Table 4. Defects produced as a result of tool design.

Tool	Kissing Bond	Flash	Tunneling Defect
A	✘	✘	✘
B	✘		
C	✘		
D			✘
E, F and G	Defect-free		

The elongation, yield strength and ultimate tensile strength in the as-weld condition are shown in Figure 3. While negligible differences in the ultimate tensile strength were found for the different tool designs, the tool F joint demonstrates a higher yield strength and elongation. Therefore, the tool F joint is an optimized tool design for the FSW of AA2024 and AA2198.

← AA 2024-RS
TD

AA 2198-AS →
RD

(a)



(b)



(c)

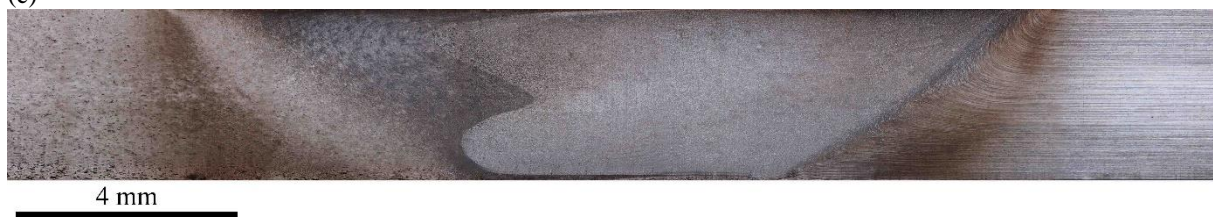


Figure 2. Cross-section observations of joints between AA2198 and AA2024 by: (a) tool E (Fan shoulder with cylindrical pin), (b) tool F (Fan shoulder with tapered cylindrical pin), and (c) tool G (Fan shoulder with cubic pin).

All tensile specimens of samples produced by tool E and G failed on the advancing side (AA2198) in the heat affected zone (HAZ) area. Some samples produced by tool F failed on the advancing side (AA2198) in TMAZ and some others in the middle of the joint. Both fracture modes are shown in Figure 4. Strain maps in the principal loading direction obtained from digital image correlation (DIC) results for the joint produced by tool F are depicted in Figure 5 at various stress levels (260, 300 and 340 MPa). Strain localizes on the advancing side (AA2198) in the TMAZ and at the center of the joint, both areas are fracture locations. Interestingly, strain localizes earlier at the TMAZ region than at the center of the joint (see *e.g.* Figure 5 at 260 MPa). For comparison, the micro-hardness

map of this sample is shown in Figure 6. The two fracture locations and strain localization regions correspond to the area with the lowest hardness values. Lower local mechanical properties are commonly reported for the TMAZ/HAZ regions [16, 17]. Therefore, damage formation under monotonic loading and fracture may occur there. Nevertheless, fracture in the middle of the joint in the area with lower hardness needs more investigation and research.

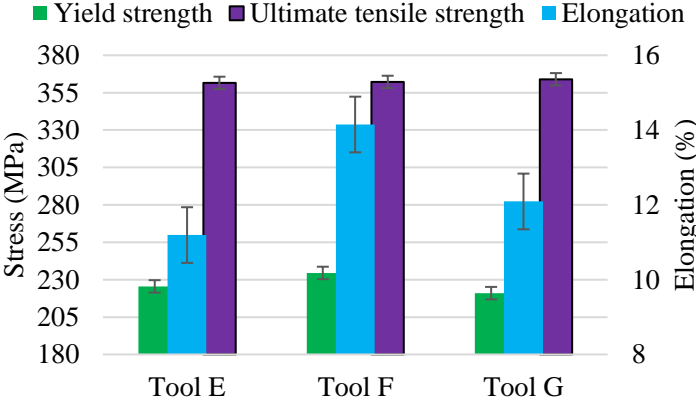


Figure 3. Mechanical properties of FSW joints produced by tool E, F and G at 750 rpm and 50 mm/min.



Figure 4. Fracture locations after monotonic tensile tests found in the middle of the joint or on the advancing side in the TMAZ. a) tool F, b) tool G.

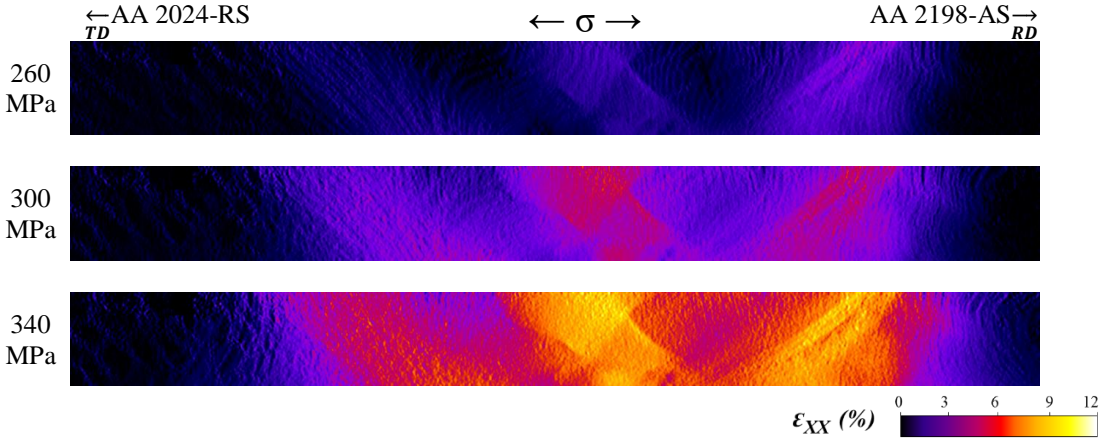


Figure 5. Local in-plane strain distribution obtained with DIC for joint produced by tool F (ω 750V50) corresponding to Figure 2-b.

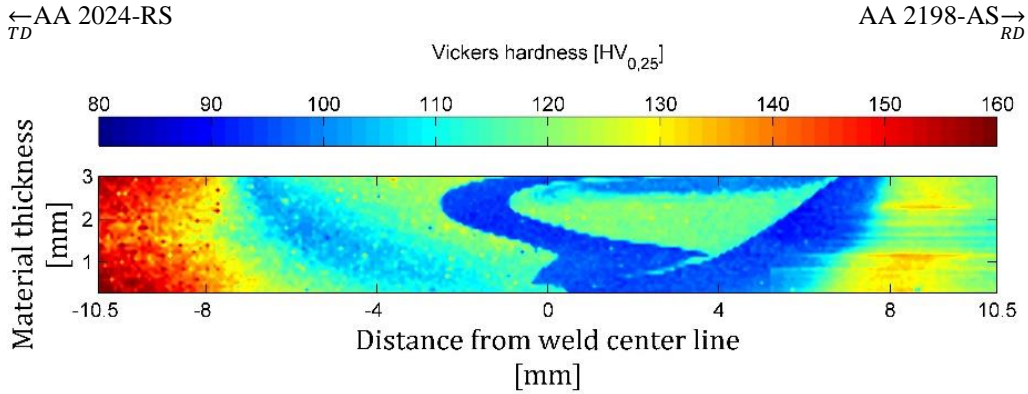


Figure 6. Micro hardness map of sample $\omega 750V50$ produced by tool F.

3.2. Welding speed optimization for selected tool

Macrograph analysis was conducted on the joints produced using tool F and welding parameters mentioned in Table 3. The tunneling defects were found only in the joint with highest rotational speed (1000 rpm) and highest traverse speed (450 mm/min), as shown in Figure 7. These findings are in agreement with those of other researchers who reported that have stated that increasing the rotational speed raises the possibility of tunneling defects. All the samples welded at traverse speed higher than 150 mm/min contain kissing bond defects because the weld is not hot enough to allow material flow in the root of the weld. Thus, it can be concluded that the tool length has to be increased at higher welding speeds to avoid the formation of kissing bond defect. The mechanical properties of FSW joint with different welding speeds is shown in Figure 8. Sample $\omega 1000V450$ has the lowest elongation and ultimate tensile strength due to tunneling defect despite a relatively good yield strength compared to other conditions.

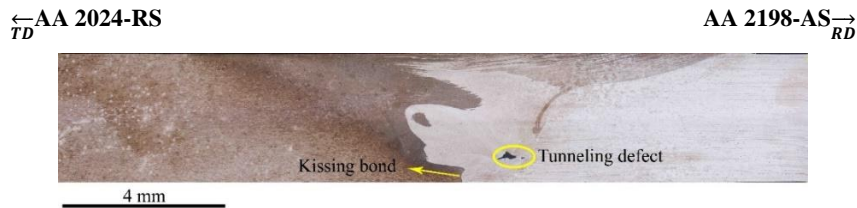


Figure 7. Cross-sectional observations of joint produced by tool F at 750 rpm and 450 mm/min welding speed which contain tunneling and kissing bond defects.

Figure 8 demonstrates that increasing rotational speed from 750 rpm to 1000 rpm with the same traverse speed (300 mm/min) has no significant effect on the mechanical properties of the joint. This result is in good agreement with investigations done by Dubourge *et. al.* [25]. As depicted in Figure 8, with the same rotational speed (750 rpm), increasing the traverse speed from 50 mm/min to 450 mm/min increases the joint yield strength. This latter result is consistent with a previous study on AA2198-T8 [26]. Results also show that the optimum rotational and traverse speeds to achieve the highest yield strength are 750 rpm and 450mm/min, respectively. The joint efficiency (the ratio between yield strength of the joint compared to the weakest base metal) has shown in Figure 9. Results indicate that an increase from 50 mm/min to 450 mm/min at 750 rpm rotational speed can increase the joint efficiency from 63% to 78 %. The following relationship can be extracted for the weld joint efficiency as a function of welding traverse speed.

$$\text{Joint efficiency (\%)} = -8E-05V^2 + 0.0722V + 60.662$$

This power-law relationship is appropriate for traverse speed ranging from 50 mm/min to 450 mm/min. This correlation can be used for higher welding speeds as long as there is no defect due to the cold weld condition at higher speeds.

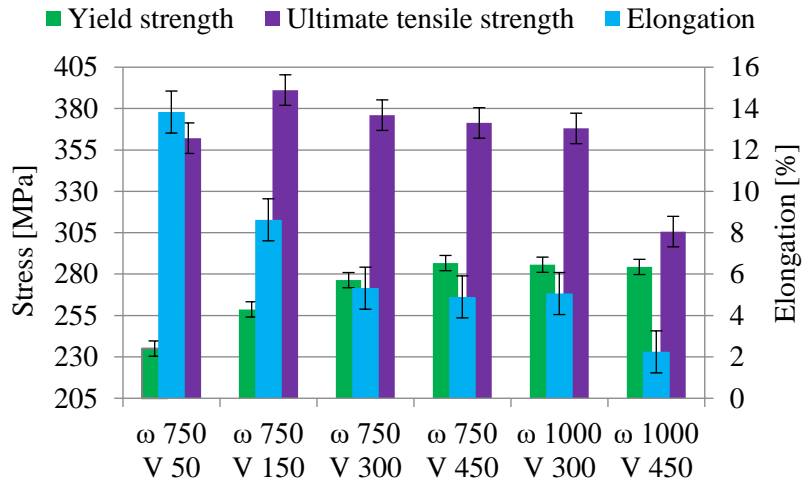


Figure 8. Mechanical properties of FSW joints produced by tool F according to welding conditions in Table 3.

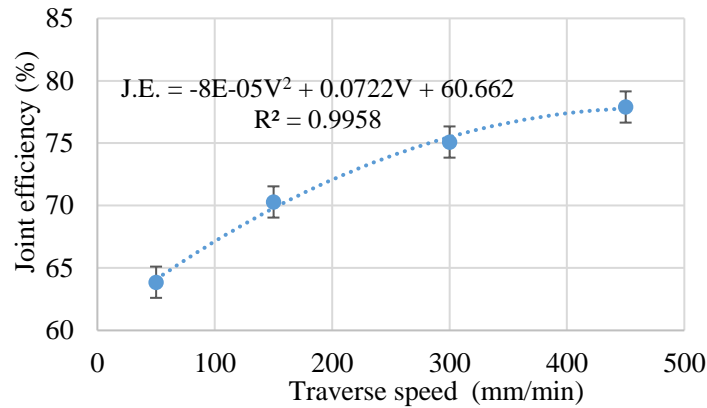


Figure 9. The joint efficiency as a function of welding traverse speed at same rotational speed 750 rpm.

4. Conclusions

The present study documents the effect of the FSW tool design and welding speed parameters on the mechanical characteristics of AA2198/AA2024 dissimilar joints. Five different pin profiles (tapered cylindrical, straight cylindrical, thread cylinder, cone and square) with three different shoulder profiles (flat, spiral, and fan) were designed and manufactured. Defect-free joints performed with these tools were characterized by means of visual inspection, microstructure analysis and tensile tests. Besides, the influences of traverse and rotational speeds on the joint efficiency have been assessed for the optimal tool. The following are the main conclusions of the study:

- (1) The tapered cylindrical pin with a fan shoulder joint exhibits higher mechanical properties for FSW of AA2198-T3 and AA2024-T3.
- (2) The optimum welding speed parameters with tapered cylindrical pin are 750 rpm and 450 mm/min for the highest yield strength. The joint efficiency can reach up to 78% of AA2198.
- (3) The probability of tunneling and kissing bond defects is higher by increasing the rotational and traverse welding speed over 750 rpm and 150 mm/min, respectively.

5. Acknowledgment

We would like to express our appreciation to Ludovic diez-jahier, Eric Marcoux and Michel Orsini for their helps during this research. Without their valuable assistance, this work would not have been completed. A part of the research presented in this paper was financed by the Fonds de recherche du Québec – Nature et technologies by the intermediary of the Aluminum Research Centre – REGAL.

6. References

1. N.D. Alexopoulos, et al., *International Journal of Fatigue*, **56**(2013): p. 95-105.
2. A. Handbook and B. Welding, ASM International, Material Park, OH,(2005): p. 438.
3. R.S. Mishra and Z. Ma, *Materials Science and Engineering: R: Reports*, **50**(2005): p. 1-78.
4. A. Scialpi, L.A.C. De Filippis, and P. Cavaliere, *Materials & Design*, **28**(2007): p. 1124-1129.
5. H.K. Mohanty, et al., *Journal of Marine Science and Application*, **11**(2012): p. 200-207.
6. L. Trueba Jr., et al., *Journal of Materials Processing Technology*, **219**(2015): p. 271-277.
7. R. Ashok Kumar and M. Thansekhar. *Advanced Materials Research*. (2014): Trans Tech Publ.
8. M.H. Idris and M.S. Husin, *Applied Mechanics and Materials*, **465**(2014): p. 1309-1313.
9. M. Reza-E-Rabby and A.P. Reynolds, *Procedia Engineering*, **90**(2014): p. 637-642.
10. S. Amini and M.R. Amiri, *The International Journal of Advanced Manufacturing Technology*,(2015): p. 1-7.
11. A. Amirafshar and H. Pouraliakbar, *Measurement*, **68**(2015): p. 111-116.
12. K. Krasnowski and S. Dymek, *Journal of Materials Engineering and Performance*, **22**(2013): p. 3818-3824.
13. Y.-h. Zhao, et al., *Materials Letters*, **59**(2005): p. 2948-2952.
14. C. Bitondo, et al., *The International Journal of Advanced Manufacturing Technology*, **53**(2011): p. 505-516.
15. I. Radisavljevic, et al., *Transactions of Nonferrous Metals Society of China*, **23**(2013): p. 3525-3539.
16. H. Robe, et al., *Materials Characterization*,(2015).
17. D. Texier, et al., *Materials & Design*, **108**(2016): p. 217-229.
18. Y. Zhang, et al., *Canadian Metallurgical Quarterly*, **51**(2012): p. 250-261.
19. E. Salari, et al., *Materials & Design*, **58**(2014): p. 381-389.
20. S. Ji, et al., *Materials*, **6**(2013): p. 5870-5877.
21. L. Kamble, S. Soman, and P. Brahmankar, *Journal of Mechanical and Civil Engineering (IOSR-JMCE)*,(2012).
22. Á. Meilinger and I. Török, *Production Processes and Systems*, **6**(2013): p. 25-34.
23. J.C. Stinville, et al., *Experimental Mechanics*, **56**(2016): p. 197-216.
24. M. Masoumi, et al. *The International Committee for Study of Bauxite, Alumina & Aluminium conference*. Quebec City, Canada. (2016).
25. L. Dubourg, R. Amargier, and M. Jahazi. *7th International Symposium on Friction Stir Welding*. Awaji Yumebutai Conference Centre, Awaji Island, Japan. (2008).
26. Y.E. Ma, et al., *Engineering Fracture Mechanics*, **114**(2013): p. 1-11.